Mesoscale Forecasting during a Field Program: Meteorological Support of the Labrador Sea Deep Convection Experiment

Ian A. Renfrew,* G. W. K. Moore,* Teddy R. Holt,+ Simon W. Chang,+ and Peter Guest#

ABSTRACT

This report discusses the design and implementation of a specialized forecasting system that was set up to support the observational component of the Labrador Sea Deep Convection Experiment. This ongoing experiment is a multidisciplinary program of observations, theory, and modeling aimed at improving our knowledge of the deep convection process in the ocean, and the air–sea interaction that forces it. The observational part of the program was centered around a cruise of the R/V *Knorr* during winter 1997, as well as several complementary meteorological research flights. To aid the planning of ship and aircraft operations a specially tailored mesoscale model was run over the Labrador Sea, with the model output postprocessed and transferred to a remote field base. The benefits of using a warm-start analysis cycle in the model are discussed. The utility of the forecasting system is illustrated through a description of the flight planning process for several cases. The forecasts proved to be invaluable both in ship operations and in putting the aircraft in the right place at the right time. In writing this narrative the authors hope to encourage the use of similar forecasting systems in the support of future field programs, something that is becoming increasingly possible with the rise in real-time numerical weather prediction.

1. Introduction

Deep convection in both the atmosphere and the ocean is an integral component of the earth's climate system. Indeed, in both fluids deep convection, that is, convection that mixes the entire fluid column, can be said to "drive" major parts of the general circulation. In the atmosphere, solar forced moist convection in the Tropics constitutes the upward branch of the Hadley cell, the dominant cell in the meridional atmospheric circulation. In the ocean, deep convection at high latitudes is responsible for an overturning that ventilates the deep ocean in a process that "sets the pace" of the oceanic thermohaline circulation. Oceanic deep convection is forced by a loss of buoyancy of the surface waters, a process that occurs through interactions between the ocean and the atmosphere. Convection takes place both near boundaries and in the open ocean, and it is the latter that we concentrate on here. Open ocean convection is thought to occur in the following manner [see Fig. 1 and Killworth (1983); Marshall and Schott (1999)]. It starts with a preconditioning phase, where a cyclonic gyre leads to a doming of isopycnals (through thermal wind balance) and therefore a weakening of the vertical stability. A consistent loss of buoyancy further preconditions the region and, eventually, leads to an erosion of the remaining mixed layer stratification. The loss of buoyancy occurs either as atmospherically forced surface cooling and evaporation, or by brine rejection as sea ice forms. At this point, violent mixing in the vertical can be triggered by further buoyancy losses forced by the passage of weather systems. The mixing is localized into columns or "plumes" of diameter about 1 km, within a larger neutral stability water column or "mixed patch." The vertical velocity in these plumes is on the order of 0.1 m s^{-1}, so with ocean basins a few kilometers deep

*Department of Physics, University of Toronto, Toronto, Ontario, Canada.
+Naval Research Laboratory, Monterey, California.
#Naval Postgraduate School, Monterey, California.
Corresponding author address: Dr. Ian A. Renfrew, British Antarctic Survey, High Cross, Madingley Road, Cambridge CB3 OET, United Kingdom.
E-mail: i.renfew@bas.ac.uk
In final form 30 November 1998.
©1999 American Meteorological Society

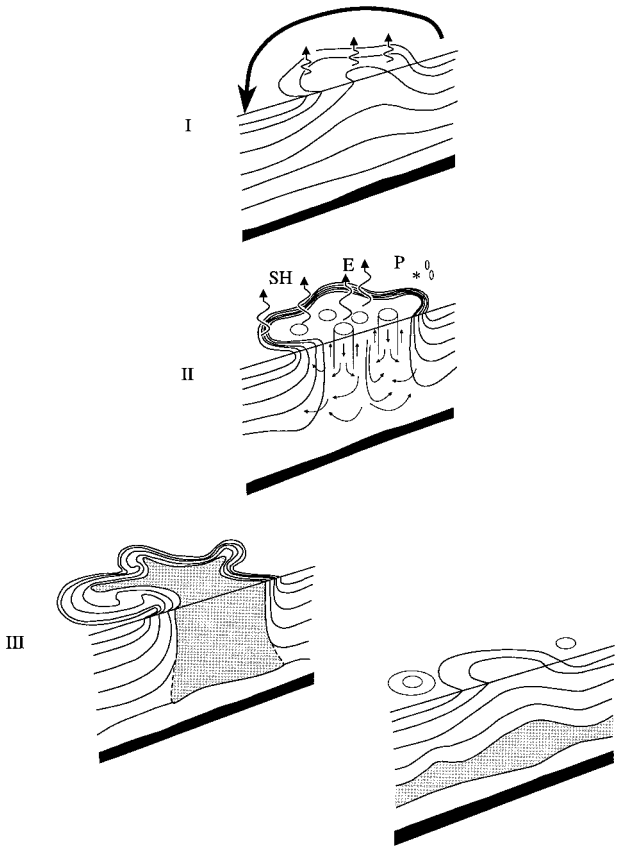

FIG. 1. A sketch of the deep convection process in the Labrador Sea. The contours represent isopyncals—surfaces of constant density. Part I shows the *preconditioning* phase. A cyclonic gyre (the Greenland and Labrador Currents) causes a doming of isopycnals, with fluxes of heat and moisture out of the oceanic mixed patch leading to a further loss of buoyancy. Part II shows the *deep convection* phase. Enhanced atmospheric forcing leads to larger air–sea fluxes and the triggering of an overturning of the ocean column. The atmospheric forcing is shown as a transfer of sensible heat (SH); evaporation (E), which both cools and increases the salinity of the surface waters; and precipitation (P), which freshens the surface waters. The vertical mixing takes place within small-scale plumes. Part III shows the *lateral exchange and spreading* phase. The shading indicates areas of the fluid that have been mixed. A lateral exchange of fluid shuts down convection (adapted from Marshall and Schott 1999).

this gives an overturning time on the order of 1 day. Hence there is an interesting temporal overlap between this fast oceanic process and synoptic-scale atmospheric processes. Following the vertical mixing there is a sinking and spreading phase as the dense water moves out laterally at some depth. There is an eventual shutdown of convection by a lateral exchange of fluid, through baroclinic instability breaking up the convective mixed patch (Killworth 1983; Visbeck et al. 1996; Marshall and Schott 1999), or mean flow advection of the plumes out of the preconditioned region (Alverson 1997), or a variety of other processes.

This discriminating set of conditions means that open ocean convection only occurs in a very limited number of places worldwide: namely, the Labrador Sea, the Greenland–Iceland–Norwegian Seas, the Mediterranean Sea, and the Weddell Sea (Killworth 1983; Marshall and Schott 1999). The first of these regions has recently been targeted as an area of intensive research, leading to the establishment of the Labrador Sea Deep Convection Experiment. This is a multidisciplinary program of meteorological and oceanic observational, theoretical, and modeling initiatives, which is ultimately aimed at "improving our understanding of the convective process in the ocean and its representation in models" (Lab Sea Group 1998). The focal point of the observational effort so far has been a 40-day cruise of the Research Vessel (R/V) *Knorr* in the winter of 1997. During the cruise a wide range of meteorological and oceanic measurements were made, and a vast array of buoys, floats, and moorings were deployed. The meteorological measurements included continuous recording of surface state variables, five to seven rawinsonde launches per day, and certain periods of high-frequency turbulent flux measurements. More details of both the oceanographic and meteorological instrumentation can be found in Lab Sea Group (1998).

The 1997 cruise was supplemented by several aircraft missions aimed at sampling the atmosphere over the Labrador Sea. The use of aircraft in the Labrador Sea Experiment allowed the measurement of, for example, the spatial distribution of surface heat fluxes over only a few hours—something that could not be obtained from the ship. The aircraft available were the C-130s of the 53d Weather Reconnaissance Squadron of the U.S. Air Force (USAF) Reserve, the "Hurricane Hunters," on a northern excursion. The aircraft could measure state variables at flight level and had dual dropsonde capabilities. They were also fitted with an additional internal fuel tank that gave a flight duration time in excess of 11 h, allowing typical flight tracks of over 4000 km. The aircraft were available on a time-sharing basis with the Fronts and Atlantic Storms Experiment (FASTEX) field experiment (e.g., Joly et al. 1997), which meant careful scheduling of aircraft missions was required.

An integral part of the Labrador Sea field work during 1997 involved the detailed planning of operational activities for both the aircraft and the R/V *Knorr*. Observing deep convection relies on knowledge of the

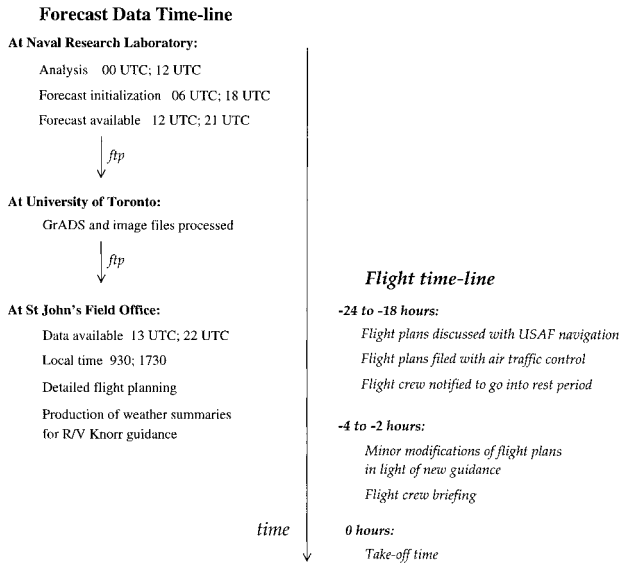

FIG. 2. A sketch of the time lines involved in the forecasting and flight planning processes.

state of the oceans, essentially where the regions of weak stability are located, and predictions of where the atmospheric forcing will be largest. Profiling floats that measured temperature and salinity (and telemetered data back in real time via satellite) had been deployed in the Labrador Sea in October 1996. These allowed a sparse map of oceanic stratification to be compiled as the fieldwork started in January 1997. The oceanographic data were combined with climatological surface heat fluxes to define a target region for oceanic and atmospheric observations, which was approximately 54°–58°N, 51°–56°W (see Fig. 10 of Lab Sea Group 1998).

One aim of the 1997 meteorological fieldwork was to sample major atmospheric forcing events in this region with a comprehensive observing system, that is, the *Knorr* surface meteorological and turbulence measurements, complemented by aircraft measurements. Analysis of such a dataset would provide much needed verification of model air–sea fluxes, a key input to oceanic models. Many of the specialized ship-based turbulence measurements, and obviously the aircraft, were only able to operate for short periods of time. Thus to obtain good observational data accurate spatial and temporal forecasts of the atmosphere were required, with enough lead time to allow coordination with the ship-based scientists, as well as flight planning, flight-track clearance, and adequate flight-crew notification. To this end, a real-time forecasting system was run at the Naval Research Laboratory (NRL) in Monterey, California, and the University of Toronto, in Ontario, Canada. The forecasting system was carefully designed to 1) provide mesoscale forecasts of the atmosphere for the Labrador Sea Experiment area; 2) provide these forecasts to the relatively remote field office in a timely manner, far enough ahead to be useful in the planning of ship and aircraft activities; and 3) provide only a limited number of specially chosen fields but at high temporal and spatial resolution, thus allowing for detailed planning without the field scientists becoming swamped with data.

The design and implementation of the forecasting system is discussed in more detail in section 2. The forecasts proved to be a tremendous asset in the day-to-day planning of scientific and ship operations aboard the *Knorr* and invaluable in flight planning for the aircraft missions. On the *Knorr*, the forecasts allowed the scheduling of delicate mooring or buoy deployment during periods forecast to be relatively calm, with the more robust hydrographic work undertaken during periods of rougher weather. The forecasting system aided the planning of three successful meteorological research flights during the 1997 season, including the comprehensive sampling by both aircraft and ship of a cold air outbreak (where surface heat fluxes are typically very high). We describe in detail the utility of the forecasting system during the flight planning process in section 3. It is worth emphasizing that the detailed information we provided was not

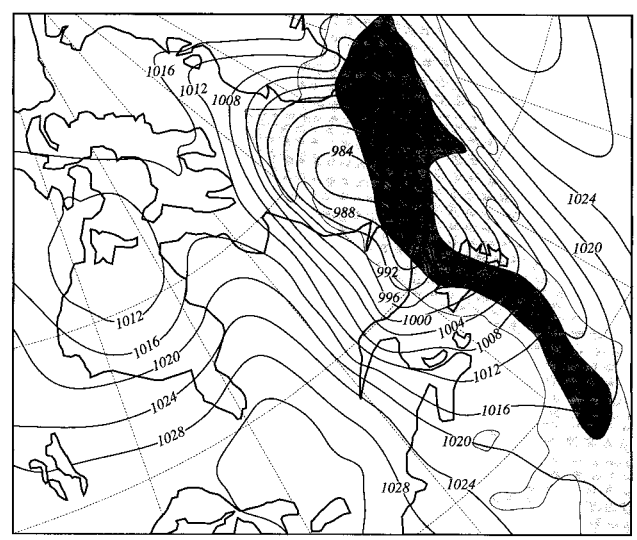

FIG. 3. Forecast of sea level pressure and precipitation for 0000 UTC 27 Jan 1997 redrawn from Environment Canada's RFE model. The contours are isobars, every 4 mb; and the shading is the 6-h accumulated precipitation: light shading 1 mm, dark shading 5 mm.

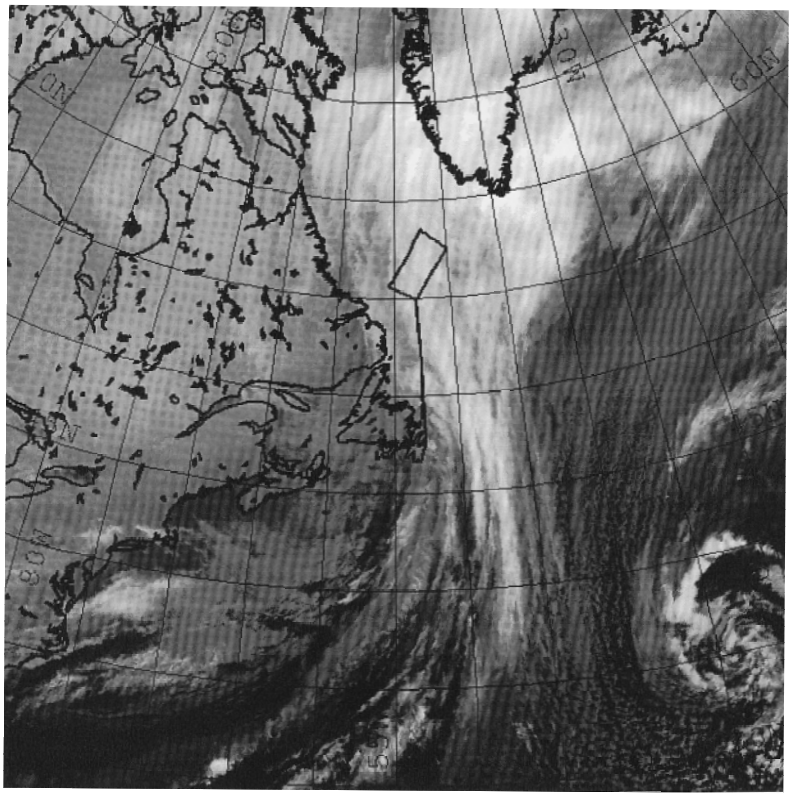

FIG. 4. *GOES-8* infrared satellite image of the western Atlantic, from 0000 UTC 27 Jan 1997. The low pressure system has a well-defined cloud head and a frontal band trailing south. The flight track of the 26–27 Jan mission is superimposed on the image.

available through operational channels. The relative remoteness of the Labrador Sea meant it was outside the domains of most operational regional-scale models, and in any case these operational centers do not provide the luxury of the tailored forecast output we had designed. The aim of this paper, then, is to detail the real-time forecasting system set up for the Labrador Sea Experiment and illustrate its value in planning the location and timing of the 1997 observational program. We discuss the design of such a forecasting system along with our conclusions in section 4.

2. Real-time forecasting support

The real-time forecasting was centered around numerical weather predictions by the U.S. Navy's regional-scale model, the Coupled Ocean–Atmosphere Mesoscale Prediction System (COAMPS). The system was configured as a stand-alone atmospheric model for the experimental period. It has been used both as a research tool (e.g., Doyle 1995; Hodur 1997) and in previous real-time settings (Hodur 1997). During the experimental period, from January to March 1997, forecasts were made twice daily out to 36 h. In the context of a field program there is clearly a trade-off between the forecast integration period, model resolution, data postprocessing time, data transfer constraints, and the timeliness of the final forecast product. There is little use for a high-resolution forecast after the observing window has shut! Indeed, after the first few forecast runs during the preexperimental period, we realized that the planned 24-h forecasts were not going to provide sufficient lead time for our ship and flight planning, and fortunately we were able to extend the runs out to 36 h.

The domain for the real-time COAMPS regional forecasts covered the Labrador Sea region, including Atlantic Canada and Greenland (see Fig. 5). It had 81×81 grid points in the horizontal, with a 45-km grid resolution, and 30 vertical levels. The forecasts produced used the nonhydrostatic atmospheric component of COAMPS implemented in a 12-h intermittent, incremental data assimilation mode for the 3-month experimental period. An initial cold start using the navy's global spectral model Navy Operational Global Atmospheric Prediction System (NOGAPS) fields interpolated to the model domain as first guess fields was performed on 2 January 1997. Subsequent forecasts used COAMPS 12-h forecasts as first-guess fields for the multivariate optimum interpolation analysis scheme. Note the use of this "warm"-start analysis cycle is markedly different from the cold starts used by most other nonoperational forecasting efforts (e.g., Mass and Kuo 1998). This approach has the advantage of initializing the forecast with data that are inherently more compatible, as they have been generated by the same model, at the same resolution, and with the same parameterizations. It means that mesoscale details and parameterized quantities should be more easily retained and more accurate through each forecast cycle (Hodur 1987, 1997). For the model setup implemented here, horizontal and vertical winds, temperature, pressure, and all water variables were warm started. Model drift was not thought to be a problem for this region. Data used in the analysis included wind

observations obtained from rawinsondes, pilot balloons, standard aircraft reports, high-frequency aircraft reports, passive microwave satellite data [Special Sensor Microwave/Imager (SSM/I)], surface, and cloud track winds. Height and thickness observations obtained were from rawinsondes, and Defense Meteorological Satellite Program and National Oceanic and Atmospheric Administration (NOAA) satellites. Quality control algorithms developed by Baker (1992) were used to screen data for their integrity and representativeness. Separate univariate temperature and dewpoint depression analyses were also performed and blended with the multivariate height and wind analyses. Lateral boundary conditions at 3-h intervals were provided by concurrent NOGAPS forecasts. The sea-ice mask was updated daily with an optimum interpolation analysis scheme using SSM/I data. The ice concentration was taken as 100% up to the ice edge. To investigate air–sea interaction processes, the planetary boundary layer parameterization is crucial; the operational version of COAMPS ran with the predictive turbulent kinetic energy scheme following Mellor and Yamada (1974). An in-depth description of COAMPS is available in Hodur (1997).

A simple distributed forecasting system was set up (e.g., Powers et al. 1997) using facilities at the Fleet Numerical Meteorology and Oceanography Center (FNMOC)/NRL complex in Monterey, California; the University of Toronto, Ontario; and at the field base in St. John's, Newfoundland. The 36-h COAMPS forecasts were run using six processors on the FNMOC Cray C90, requiring approximately 24 Mwords of memory and a total of 40 min of CPU time. The model fields were output in both graphical format, at 12-h time resolution, and as binary files, at 1-h time resolution. These files were then copied by an automatic ftp-script over the Internet to the Department of Physics at the University of Toronto. Here a limited amount of postprocessing was carried out. The graphics files were pared into three batches of image files, and the binary data were translated into a format readable by the GrADS graphics package (http://grads.iges.org/grads). These files were then transferred via ftp to the field base at the St. John's Weather Centre, at St. John's Airport in Newfoundland. The image files were used in the basic flight planning and in the production of general forecasts for the Labrador Sea. The timing and location of field activities were then refined after examining the hourly data with GrADS.

Figure 2 outlines the time lines of the forecasting and planning procedures. The forecasts were initiated at FNMOC/NRL at 0600 and 1800 UTC and were available at NRL at 1200 and 2100 UTC for the 0000 and 1200 UTC analysis times, respectively. The difference in arrival times (6 vs 3 h) was due to scheduling differences of navy operational runs on the Cray C90. The Labrador Sea COAMPS run was scheduled with a lower priority than the operational jobs. Transferring large amounts of data over the Internet can be prohibitively slow, as discussed by Mass and Kuo (1998) and Powers et al. (1997), and therefore it has to be carefully planned. A crucial decision in the design stage was to limit the number of fields transferred to only a dozen or so two-dimensional surface and 500-mb fields. This sped up the postprocessing and ftp times considerably, mean-

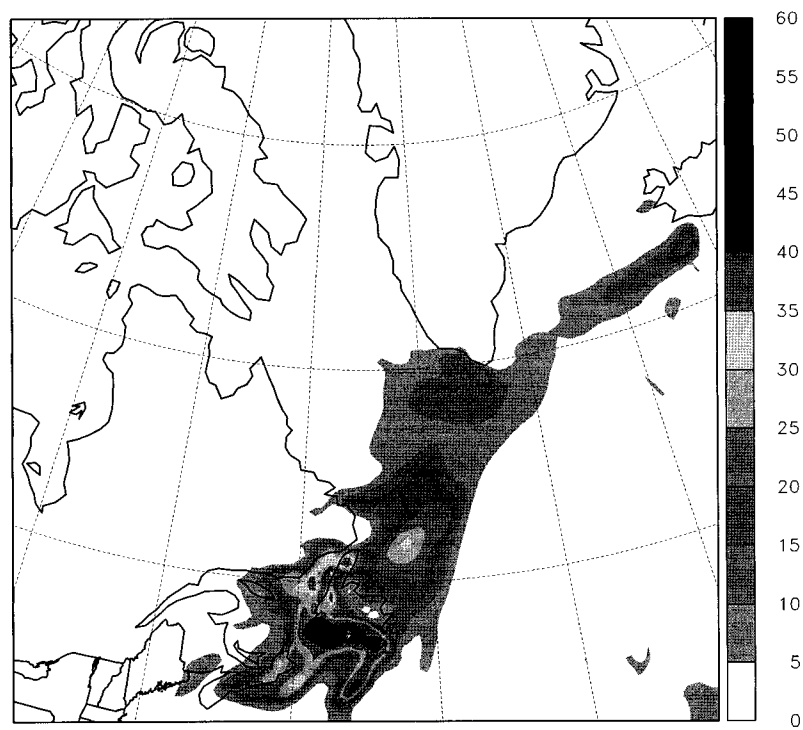

FIG. 5. Precipitation forecasts from the COAMPS model for 0000 UTC 27 Jan. Accumulated precipitation (mm) over 24 h is shown for both a warm start (shading) and a cold start (contour) from 0000 UTC 26 Jan. The cold start forecast fails to generate a frontal rainband.

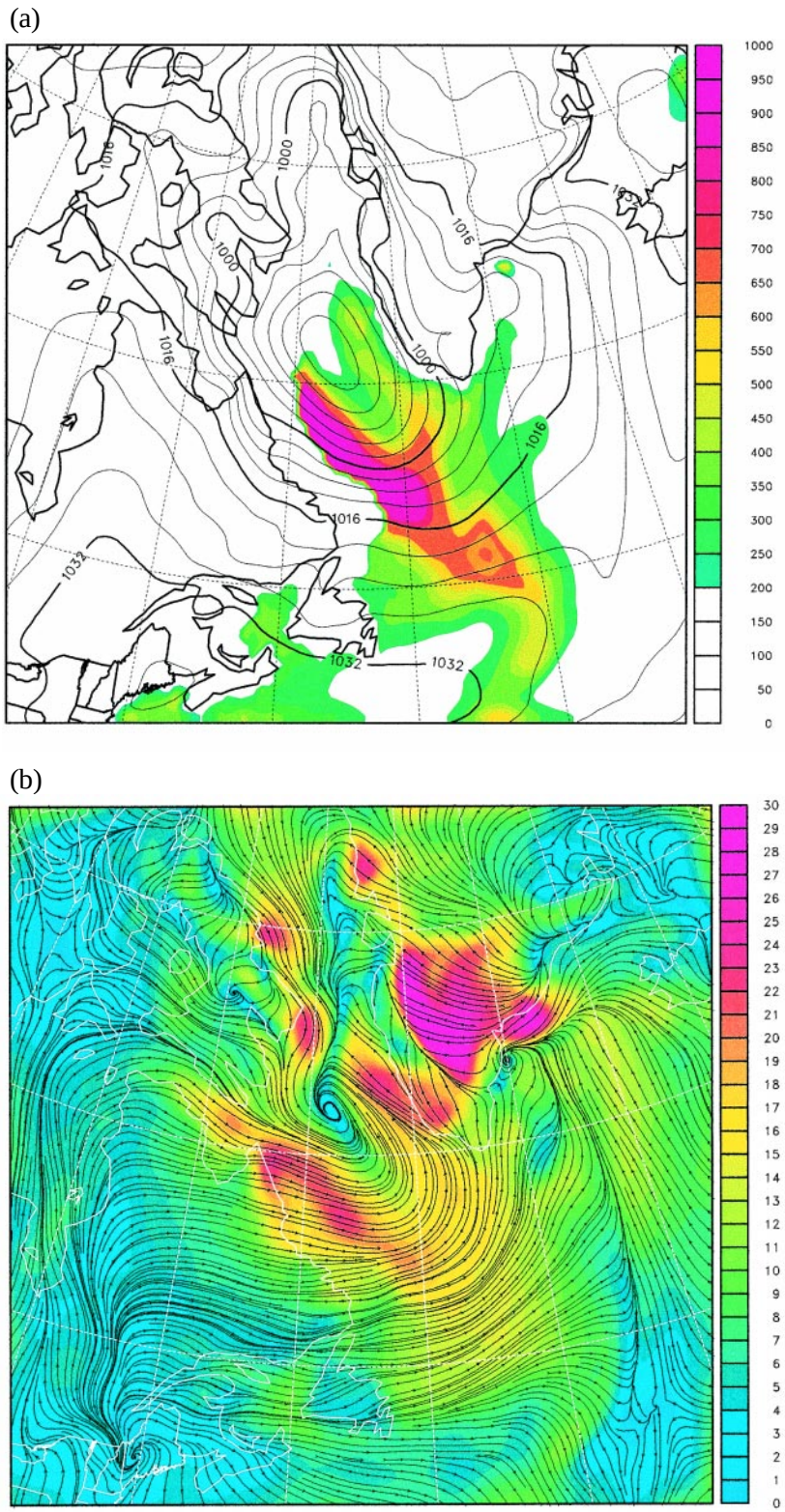

FIG. 6. (a) Forecast of sea level pressure (contours every 4 mb) and surface total (sensible plus latent) heat flux (color bar in W m^{-2}) at 2100 UTC 30 Jan 1997. (b) Forecast of the 10-m streamlines and wind speed (color bar in m s^{-1}) at 2100 UTC 30 Jan. Both forecasts are from the operational COAMPS.

ing the image and GrADS files were available only about an hour later, at 1300 and 2200 UTC, respectively, at the field office (0930 and 1730 local time in Newfoundland). This gave us approximately 24 h from the receipt of the prognostics till the end of their forecast period. Upon receipt of the forecasts there was a busy period of flight planning, discussion, and checks with other forecasts. A decision to fly, or stand-down, had to be made at least 18 h before the scheduled takeoff time. This lead time allowed the statutory crew a rest period of 16 h, as well as time to discuss the flight plan with the USAF navigation and planning team and obtain air traffic control clearance for the route. We found the time line illustrated in Fig. 2 was just sufficient to plan and implement the flight plans.

To supplement the COAMPS forecasts, several public domain forecasts were utilized. While at the St. John's Weather Centre, we benefited greatly from the suite of operational products available from Environment Canada. These included twice daily 48-h regional forecasts, daily 5-day global model forecasts, quality added analyses, sea-ice maps, and satellite imagery. Many of these products were also available from the World Wide Web (WWW), such as the regional and global model output (http://www.cmc.ec.gc.ca:80/cmc/htmls/forecasts.html). We also consulted, via the WWW, prognostics from the European Centre for Medium-Range Weather Forecasts (http://www.emwf.int/charts/charts.html), and from the National Centers for Environmental Prediction (http://wxp.atms.purdue.edu). In addition, a number of extraordinary forecasting products were available over the North Atlantic sector due to the FASTEX experiment; for example, forecasts and adjoint sensitivity products from NOGAPS, easily accessible

geostationary satellite imagery, and synoptic discussions from the FASTEX field office.

To aid the planning of scientific activities on board the R/V *Knorr,* forecast information was transmitted in the form of daily "weather summaries" sent by e-mail from either the St. John's field base or the University of Toronto. These e-mail summaries described the immediate upcoming atmospheric conditions for the location of the ship, emphasizing quantitative details (such as 10-m wind speed and air temperature) that were not available through the ship's normal meteorological service. A 3–5-day synoptic outlook was also included, written after consulting the global forecast products mentioned above. Also benefiting from these e-mail weather summaries was an aircraft-based remote sensing calibration program, which was coordinating overpasses with the *Knorr* (see Lab Sea Group 1998 for more details).

In summary, our field base at St. John's, Newfoundland, was well catered for, although it only consisted of a couple of PCs, a printer, and a connection to the Internet. We had access to both detailed mesoscale forecasts of the Labrador Sea and a number of medium-term standard forecast products. The exclusive numerical weather prediction carried out by NRL allowed us to tailor the model output specifically for the flight planning and ship operations planning. This meant as well as several standard forecast products, such as sea level pressure and 500-mb height fields, a select number of nonstandard fields were produced, for example, 10-m winds, surface sensible and latent heat fluxes, stable and convective precipitation, surface radiative flux components, and surface wind stress. In the next section we illustrate how these additional data helped with the nontrivial task of being in the right place at the right time.

3. Flight planning

We shall illustrate the pertinence of the forecasting support system by describing several of the meteorological aircraft missions planned during the 1997 field season of the Labrador Sea Experiment. The first aircraft mission was that of 26–27 January, flying into the precipitating region ahead of a synoptic-scale low pressure system as it tracked north into the Labrador Sea. Figure 3 shows the sea level pressure and precipitation fields at 0000 UTC on 27 January, as forecast by Environment Canada's Regional Finite Element (RFE) model. Unfortunately the COAMPS forecasts were unavailable for the planning of this mission. The COAMPS update cycle was broken at FNMOC due to unrelated problems, and the forecasts from 0000 and 1200 UTC 25 January were not produced. Such an interruption only occurred once during the experimental period, but unfortunately it was the day before a mission! It meant that for this case we had to rely primarily on the operational products from the RFE model.

A flight was planned to explore the precipitation field in the warm sector ahead of the system's low pressure center. Moore et al. (1999, personal communication) have recently shown the importance that precipitation can play in freshening surface waters and thus reducing the density of the mixed layer. This atmospheric haline forcing is thought to play a major but transient role in the forcing of ocean convection that has often been neglected in past convection studies. Although note that if the precipitation fell as snow, which is usual at this time of year, there is a counterbalancing oceanic heat loss (a density gain) associated with the phase change that occurs when the snow lying on the ocean's surface melts. The flight track is superimposed on an infrared satellite image from 0000 UTC 27 January 1997 (Fig. 4), which has been processed with colder brightness temperatures lighter. The aircraft took off at 2100 UTC on 26 January and was in the "box" part of the flight track between 2230 UTC 26 January and 0400 UTC 27 January. The flight was planned so that we could calculate the atmospheric moisture transport into the atmospheric "column" defined by the box part of the flight track. The box was circuited twice, with flight-level data recorded and dropsondes released at the corner points and on the long sides of the box. From conservation of water vapor, any moisture convergence into the column would result in either an increase in the water vapor stored in the column, and/or precipitation at the surface. By virtue of the mission design we have been able to partition the moisture convergence into these two components. Preliminary results qualitatively confirm the RFE forecast of significant precipitation in the box.

After the break in the COAMPS assimilation cycle, another cold start was required using NOGAPS fields at 0000 UTC 26 January. It is interesting that the precipitation field forecast from this cold start was radically different from the RFE forecast, with almost zero precipitation forecast over the first 24 h; that is, from a cold start the COAMPS model was unable to generate a frontal rainband for this case. To investigate this

further, a warm-start forecast, from the same analysis time of 0000 UTC 26 January, has been made. The missing forecasts from 25 January were run from a warm start at 0000 UTC, thus allowing a warm-start analysis cycle for the 0000 UTC 26 January forecast. Figure 5 shows the accumulated precipitation after 24 h, at 0000 UTC 27 January, for both warm- and cold-start COAMPS forecasts. The cold-start precipitation field has only a small area of 5-mm accumulation in the southwest corner of Newfoundland. In contrast, the warm-start precipitation field has an extensive rainband stretching from Nova Scotia to Iceland. There are between 5 and 20 mm of accumulation along most of the rainband, with the pattern and magnitude broadly consistent with the 6-h accumulation of the RFE forecast shown in Fig. 3. The COAMPS forecast produces greatly enhanced orographic precipitation, compared to the RFE, with peak values over 60 mm over southern Newfoundland. Such large amounts of orographic precipitation were noted in COAMPS forecasts throughout the experimental period. One can speculate that the relative remoteness of the region is a contributing factor to the poor performance of the COAMPS model under the cold-start conditions; however, a more thorough investigation is beyond the bounds of this report. This case does serve to illustrate the known advantages of an incremental or warm-start data analysis cycle in forecasting parameterized fields (e.g., see Hodur 1987, 1997).

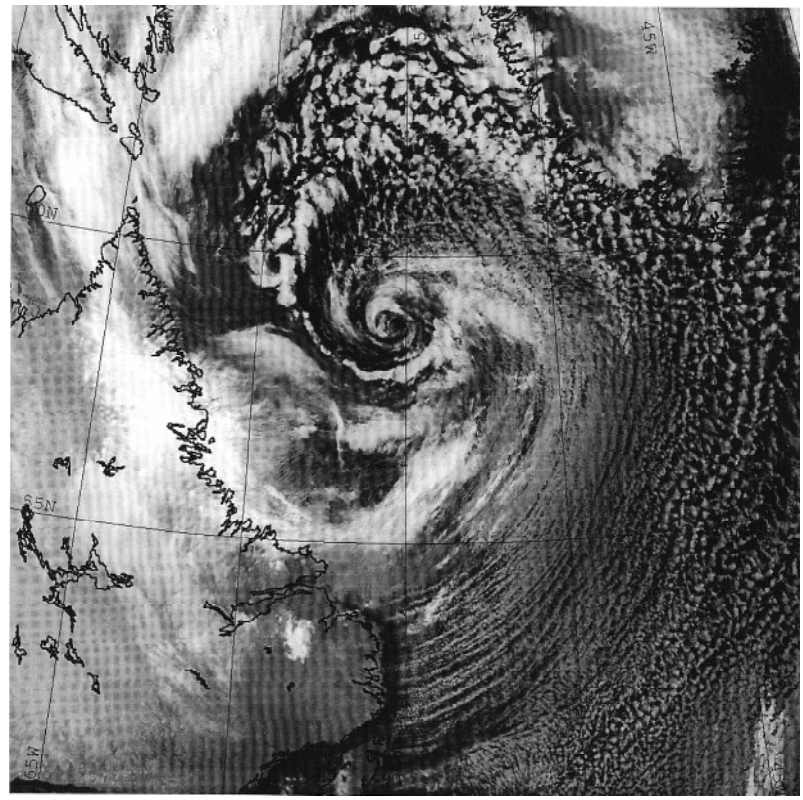

FIG. 7. (a) AVHRR infrared satellite image of the Labrador Sea region from *NOAA-12* at 2103 UTC 30 Jan 1997. A low pressure system fills the Labrador basin; there are high clouds to the west, cellular convection dotting the north and east, and cloud streets curving into the vortex center in the cold air to the south.

Our second aircraft mission was planned to fly into the cold air behind the passage of a major low pressure system that followed a similar northerly track into the Labrador Sea during 29–30 January. The idea was to fly at low levels, in the atmospheric boundary layer, to measure the large fluxes of heat and moisture from the ocean into the very cold and dry air swept off Labrador in the wake of the low. Figures 6 and 7 depict various aspects of the cyclone structure. Figure 6a plots the sea level pressure field and the total surface (sensible plus latent) heat fluxes, and Fig. 6b shows the 10-m streamlines and wind speed, both forecast from 1200 UTC 29 January and valid at 2100 UTC 30 January. Figure 6a shows a deep low pressure system filling the Labrador Sea, with a center of 980 mb located at 61°N, 55°W. An area of high surface fluxes (over 800 W m^{-2}) lies to the south, in a band along the edge of the sea ice. This region of enhanced fluxes is included in the region of high wind speeds in Fig. 6b, although they are not coincident, as areas of high wind speed over land, or sea ice, do not yield high surface fluxes. It is interesting to note that the zone of forecast high wind speeds is mainly to the south of the streamline vortex, that is, to the south of the low pressure center. Figure 7a shows an infrared Advanced Very High Resolution Radiometer (AVHRR) satellite image from 2103 UTC 30 January, received and processed at the University of Toronto. The bright clouds to the northwest and west of the low center indicate cold (high) cloud cover. To the north and east, cellular convection speckles the image, while to the immediate south and southeast the convection is formed into distinctive "cloud streets," with occasional areas of higher cirrus cloud overlying. The shallow convection in the image is indicative of an unstable boundary

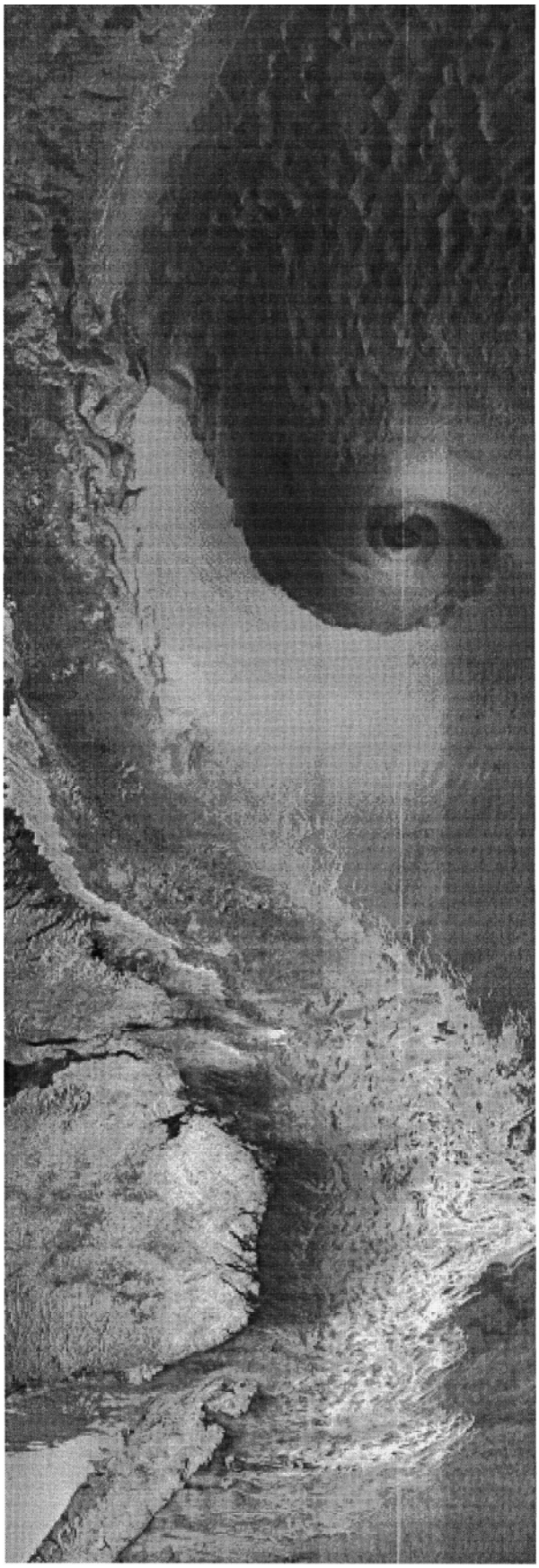

layer, presumably caused by air–sea interaction as the very cold, dry air moves over the relatively warm ocean. Figure 7b is a Radarsat Synthetic Aperture Radar (SAR) image received and processed by the Canadian Space Agency at 2130 UTC 30 January. Over the ocean, SAR is sensitive to changes in the surface roughness, so it primarily reflects changes in surface wind speed and direction (e.g., Alpers and Brümmer 1994). The extremely high resolution of the data (in this case 100 m by 100 m) means that surface wind patterns induced by mesoscale atmospheric phenomena may be easily detected. This image has been processed such that white represents high radar reflectivity, caused by a rough sea surface from high surface wind speeds. The image clearly shows the vortex evident in Figs. 6 and 7a. Note there is a striking difference in reflectivity to the north and south of the vortex center. The sharp change in reflectivity is a combination of a change in wind speed and wind direction. To the south, the lighter region represents a swath of strong winds curving cyclonically around the vortex, and edged to the north by a well-defined line. This area of high wind speed coincides well with the forecast model wind speed shown in Fig. 6b. To the north the darker area reflects lower wind speeds, with the mottled effect caused by the cellular shallow convection that is evident in the satellite image.

A research flight into this cyclonic system was planned, with the COAMPS data used extensively for the planning. Unfortunately our plans were thwarted by mechanical problems in the aircraft. The planes were not used to the harsh Newfoundland winter weather, and one of the four engines on the allotted aircraft did not start. After a delay for some last-minute repairs, we finally had all four engines running. But then, during the last few minutes of preflight checks, a crankshaft in a different engine catastrophically failed resulting in the destruction of that engine and the termination of the mission.

Following this disappointment, however, came our third and most successful intensive observation period. Again we targeted a cold air outbreak over the south-

FIG. 7. *(continued)* (b) Radarsat Synthetic Aperture Radar image of the Labrador Sea at 2130 UTC 30 Jan. Lighter shading corresponds to high reflectivity and thus high wind speeds. A vortex is clearly seen in the image. The high wind speeds to the south match well the COAMPS forecast wind speeds in Fig. 6b. The mottled pattern to the north is the surface representation of the cellular convection seen in (a). The radarsat image is copyrighted by the Canadian Space Agency 1997.

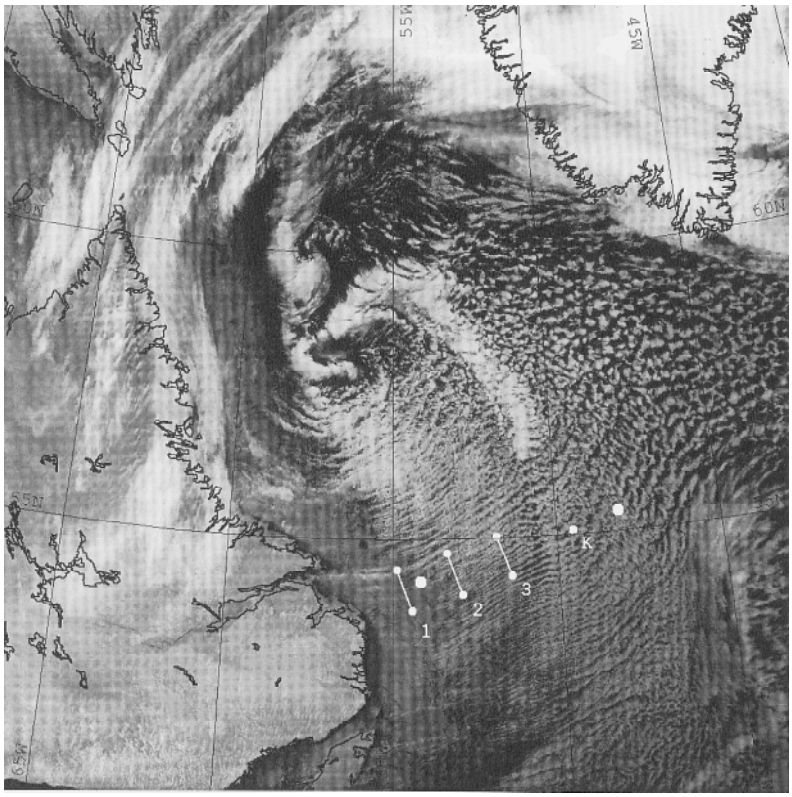

FIG. 8. AVHRR infrared satellite image from *NOAA-12* at 1119 UTC 8 Feb 1997. A low pressure system fills the image, with high clouds to the north and west. Within the low there are a number of convective cloud vortices, and a convective cloud band curving northwest–southeast. There are cloud streets over the marginal ice zone and the ice-free Labrador Sea in the cold cyclonic flow to the south. The flight plan is annotated on the image: the end points to the high-level dropsonde runs are marked as large dots; the three stacks of the low-level portion of the flight are marked 1, 2, 3; and the location of the R/V *Knorr* is marked by a K.

ern Labrador Sea, following the passage of a synoptic-scale low pressure center. The sampling of the air–sea interaction associated with this event was successful. There were two consecutive meteorological aircraft flights in the ocean convection target region (section 1) and collocated with the R/V *Knorr*. A satellite image from 1119 UTC 8 February 1997 (Fig. 8) shows a low pressure system filling the Labrador Sea basin. There is high cloud cover in the warm sector to the north of the image, and cloud streets associated with roll vortices streaming off the coast of Labrador in the cold sector to the south. Annotated on the image is the track of the high-level dropsonde leg (large white dots), which was flown twice: on the first aircraft mission between 0200 and 0400 UTC, and on the second flight between 1200 and 1400 UTC 8 February. This second flight then spiraled down to low levels to measure the surface heat and moisture fluxes into the atmospheric boundary layer between stacks 1, 2, and 3 (as marked in Fig. 8), and fly cross sections through the cloud streets. The 1200 UTC position of the *Knorr* is also shown in Fig. 8. Analysis of this case study is ongoing: observational results from the aircraft data are described in Renfrew and Moore (1999), mesoscale modeling reconstructions of the event are being carried out, and an analysis of *Knorr* meteorological data is also under way.

The low-level portion of the second aircraft flight was planned to be Lagrangian, in the sense that a hypothetical air parcel was "followed" as it was advected from over the sea ice to over the open water. An estimation of the surface heat and moisture fluxes could then be made assuming these are the primary sources to the budget equations of potential temperature and moisture; see Renfrew and Moore (1999) for further details. The Lagrangian nature of this flight plan follows that of Grossman and Betts (1990) and Bretherton and Pincus (1995). The logistics of such a Lagrangian plan are somewhat complicated. The stacks were planned with stack 1 over the sea ice, stack 2 over the marginal ice zone, and subsequent stacks downstream over the open water. Each stack consisted of three aircraft legs of 90 km in length at 170, 300, and 450 m above sea level, and flown perpendicular to the low-level wind. Note that a planned fourth stack was not flown due to mechanical problems on the C-130. The boundary layer roll vortices, which always lie roughly in the direction of the low-level wind, could then be sampled during the crosswind legs. The length of these legs was adjusted so that the elapsed time between the stacks was the same as the advection time of the hypothetical air parcel. So this flight plan depended critically on accurate forecasts of the low-level wind speed and direction. In addition to examining the roll vortices, we wanted to capture the peak surface fluxes of the cold air outbreak. This aim was greatly aided by COAMPS forecasts of the surface sensible and latent heat fluxes at 1-h resolution. Figure 9 shows a Hovmöller plot (longitude vs time) for the total surface heat flux at 54°N, starting from 0000 UTC

7 February. This forecast was available at the flight planning stage, approximately 24 h before the takeoff time. There is a sharp gradient in surface fluxes from the ice edge downstream for 50–100 km before the region of maximum fluxes is reached. One would expect a maximum in the surface sensible heat fluxes just downstream of the model ice edge, where the air–sea temperature difference is greatest. The sharp gradient reflects the abruptness of the model ice edge. Note however that the gradient has been smeared over several grid points, actually making the model forecast more like the observational data, because in reality the surface fluxes increase (with decreasing ice cover) through the marginal ice zone, which is typically 50–100 km wide (Renfrew and Moore 1999). The surface latent fluxes often appear to have a broader region of high fluxes (Renfrew and Moore 1999), as the warmer downstream boundary layer can hold a greater amount of water vapor. Figure 9 indicates the total surface fluxes were forecast to increase steadily over 7 February, reaching peak values toward the end of the forecast period between 0600 and 1200 UTC 8 February. This was corroborated by subsequent forecasts that showed the surface fluxes increasing steadily from 0000 to 1200 UTC 8 February and remaining high through the following 24 h.

Having such flux evolution maps in the field allowed us to plan with confidence the location and timing of the aircraft missions. The region of forecast peak fluxes (54°N at 48°–52°W; Fig. 9) was within the target area of weak oceanic stability noted earlier and was forecast to have low-level winds roughly perpendicular to the ice edge. To carry out the low-level part of the mission in daylight, a target time of 1200 UTC 8 February was chosen to begin the dropsonde leg. This meant a takeoff time of 1000 UTC, with the crew briefing starting 2 h previous to that, and the crew rest starting 16 h earlier. The previous aircraft mission, shared with the FASTEX experiment, was coordinated to fly the same dropsonde leg (Fig. 8) 10 h prior to the main mission between 0200 and 0400 UTC 8 February, thus allowing the evolution of the cold air outbreak to be observed. For further details on this case and an analysis of the aircraft observations, see Renfrew and Moore (1999).

Figure 10 compares hourly COAMPS forecast data with in situ observations from the R/V *Knorr* and C-130 aircraft. Figure 10a plots the sea–air temperature difference ($T_s - T_a$) through the cold air outbreak, from 1200 UTC 7 February to 2400 UTC 8 February. The COAMPS data are from three sequential forecasts

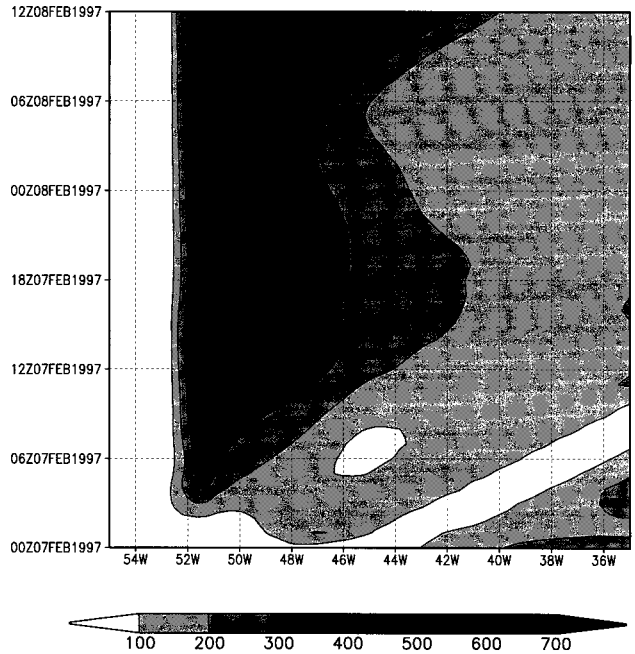

FIG. 9. Hovmöller diagram [longitude (west) vs time] of total surface heat flux (W m^{-2}) from 0000 UTC 7 Feb 1997. The data are operational COAMPS forecasts and have been visualized via the GrADS software package. This forecast was available during the planning of the 8 Feb flights.

starting at 0000 UTC 7 February, 1200 UTC 7 February, and 0000 UTC 8 February, extracted at 55°N, 50°W. There is a steady increase in $T_s - T_a$ over the period, with a small variation of 1°–2°C between the forecasts. There are some model spinup problems, with T_a too warm in the first hour or two of all the forecasts. The *Knorr* data is plotted as a line. The same general cold air outbreak signature of increasing $T_s - T_a$ is clear for both datasets. The *Knorr* was approximately stationary at 55°N, 50°W between 1200 and 2100 UTC 8 February; prior to this it was transiting from the south, which probably accounts for the lower $T_s - T_a$ values over the first part of the period. While we have some reservations in comparing point observations with gridpoint model data, it is worth noting that during the period when the ship was stationary, the model and *Knorr* data do correspond reasonably well. Two successive forecasts bracket the *Knorr* data between 1200 and 1700 UTC, after which the model air temperature is too warm by 1°–2°C. Figure 10b shows 10-m wind speed data for just the period when the *Knorr* was stationary, from 1200 to 2100 UTC 8 February. The COAMPS forecasts are from 1200 UTC 7 February and 0000 UTC 8 February. The wind speeds compare well for the period, and the later forecast even manages to reproduce the overall trend of

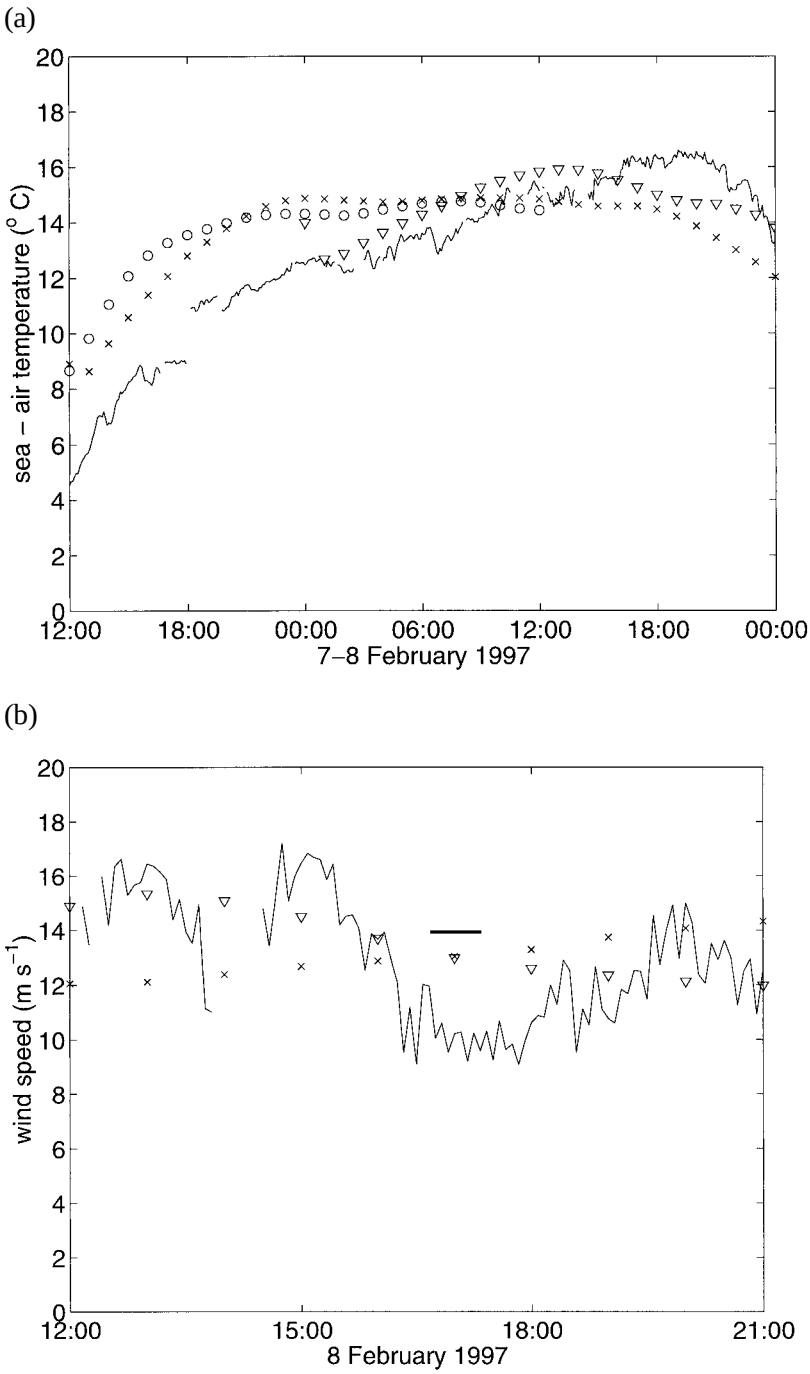

FIG. 10. (a) A time series of the sea–air temperature difference on 7–8 Feb 1997, from the R/V *Knorr* (thin line) and extracted from three successive COAMPS forecasts at 0000 UTC 7 Feb (o's), 1200 UTC 7 Feb (x's), and 0000 UTC 8 Feb (∇'s) at 55°N, 50°W. (b) A time series of wind speed on 8 Feb, from the R/V *Knorr* and COAMPS forecasts as above, as well as the mean boundary layer wind speed from stack 3 of the aircraft flight (thick line).

decreasing wind speed over the 9 h. However, in general, the short-term variability in the wind speed is not captured, illustrating the limitations of mesoscale modeling in relatively data-sparse regions. Overlaid on the wind speed picture is the mean wind speed from stack 3 of the low-level part of the aircraft flight, which is about 100 km to the west (Fig. 8). Note it is an average wind speed over all three heights (170–450 m), so a direct comparison with the other 10-m wind speeds is not really applicable. However, given the decrease in wind speed through the surface layer, it is consistent with the *Knorr* observations and the COAMPS data. These two plots give an indication of the model's usefulness and limitations in forecasting the surface fields that determine its parameterized air–sea interaction. A detailed examination of various models' parameterized air–sea interaction, using observations of surface sensible and latent heat fluxes as verification, is currently under way by members of the Labrador Sea Experiment group.

The low-level flight of 8 February was, as far as we know, the first such meteorological research flight in the Labrador Sea region. It was a visually extraordinary experience with a variety of beautiful as well as scientifically interesting sights. Three photographs have been reproduced in Fig. 11 to give a visual record of the flight. Figure 11a was taken over the near-solid sea-ice cover, at the 170-m level of stack 1, where there was little cloud cover (Fig. 8). The sea ice appears as a giant jigsaw puzzle made up of ice plates of varying sizes, from tens to hundreds of meters. Small leads are visible in the ice cover, the one nearest the camera being partially refrozen. Movement of the ice plates has caused the well-defined pressure ridges that can be seen around the edges of the plates. Farther downstream, Fig. 11b shows the marginal ice zone, with around 30%–50% ice cover. The plates of ice vary in both size (tens to hundreds of meters) and in thickness; in fact, some of the larger plates have smaller plates resting on top of them. Some major leads now break up the ice cover. In the open wa-

ter one can see small-scale ridging marked out by wave crests, approximately perpendicular to the low-level wind direction. One can also see a similar ridging in the fresh snow on top of the more stable areas of sea ice, approximately perpendicular to the prevailing wind direction. In the direction of the near-surface wind there are grayish streaks of frazil ice at, or near, the water's surface. These small ice particles act as tracers to the near-surface currents, and the streaks are thought to delineate lines of convergence formed by Langmuir cells. Figure 11c was taken farther downstream again, at the edge of the marginal ice zone, at around 10%–30% ice cover. Langmuir cells are again clearly shown by the streaks of ice particles. There is condensate visible, the water being evaporated from the ocean and then almost immediately condensed out of the very cold air. The condensate or "frost smoke" (Cherry-Garrad 1922) was often lined up in streets in the direction of the low-level wind. These frost smoke streets can be thought of as minuscule cloud streets, analogous to those formed by the shallow convection clouds that could be seen from above at higher altitudes during the flight, and in the satellite image of Fig. 8.

4. Conclusions

The purpose of this paper has been to illustrate the utility of a specialized real-time forecasting system in the operation of a remotely located field program. The atmospheric forecasting support was centered around specially tailored runs of the COAMPS model produced at the NRL/FNMOC complex in Monterey, processed at the University of Toronto, and used in the field base in St. John's, Newfoundland. The model data were transferred over the Internet. The forecasting process also benefited from a number of other World Wide Web products obtained over the Internet. The model forecasts proved to be invaluable in planning several aircraft missions, including the comprehensive sampling of an archetypal cold air outbreak over the Labrador Sea. Thus obtaining the first aircraft observations of air–sea interaction in the region. In addition, the model forecasts were used to prepare daily weather summaries, which were then e-mailed to the R/V *Knorr* in the Labrador Sea. These proved to be a real asset in the day-to-day planning of onboard operations. To quote the *Knorr's* chief scientist, "[the forecasts] helped the science party anticipate what to expect in terms of atmospheric forcing, and in planning shipboard operations, and because of the remoteness of the region, the bridge came to rely on this information as well. You should be pleased to know that the captain regularly exclaimed how much more accurate your forecasts were than the standard products they were receiving on the bridge" (R. Pickart 1997, personal communication).

In recent years, the availability of relatively inexpensive computing power and a concomitant develop-

(a)

FIG. 11. Three photographs from the low-level 8 Feb flight; see Fig. 8 for location. (a) Over the sea ice, taken during the 170-m leg of stack 1, with the camera pointing west. The photo shows a jigsaw puzzle of ice plates, with pressure ridging visible on the edges of the plates, and a few leads in the ice cover. (b, next page) The marginal ice zone, taken during the descent, with the camera pointing northwest. The ice cover is around 50%, with ice plates tens to hundreds of meters in size. On the water's surface, waves can be seen lined up perpendicular to the low-level wind direction (which is approximately from the west). (c, next page) At the ice edge, taken from the 170-m leg of stack 2, with the camera pointing east. Langmuir cells are delineated by the convergence of small ice particles in the surface ocean, lined up approximately in the direction of the low-level wind (from the west). The condensate or frost smoke is also lined up into streets in this direction.

(b)

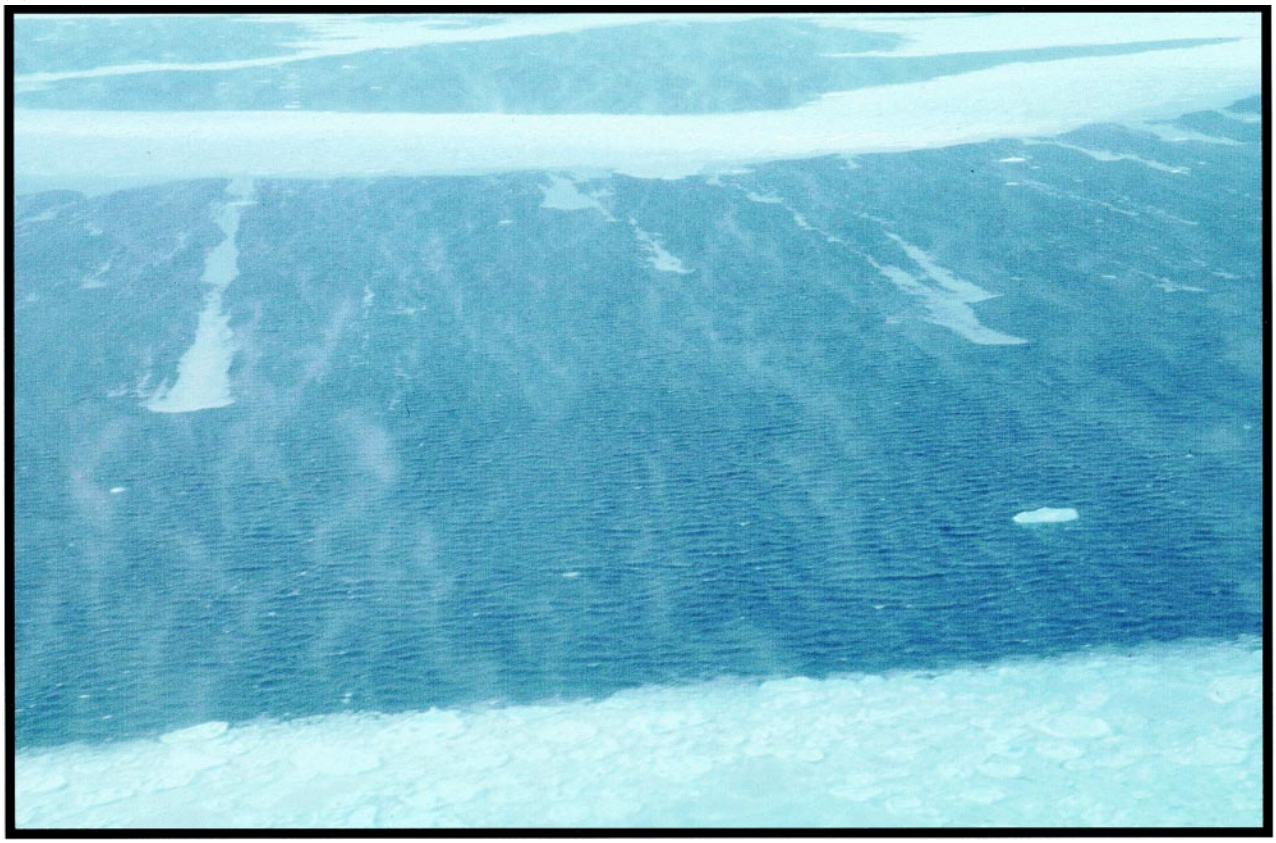

(c)

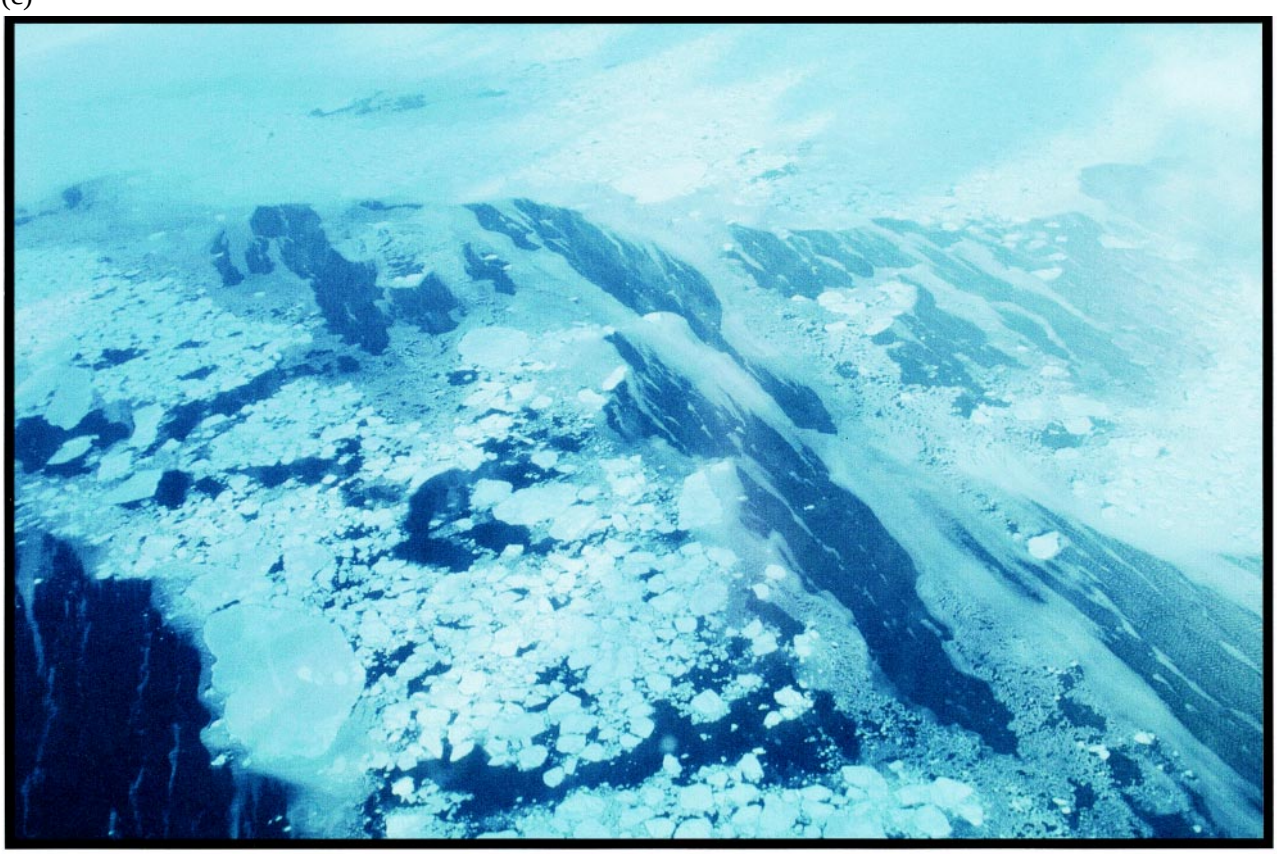

ment in the portability of atmospheric modeling systems has lead to a number of real-time forecasting efforts being established (Warner and Seaman 1990; Cotton et al. 1994; Mass and Kuo 1998). This rise in nonoperational "home forecasting" by universities and other research establishments now means the sort of support provided for the Labrador Sea Experiment could be provided by other small research groups, using one of a number of well-established mesoscale models (e.g., see Mass and Kuo 1998). One advantage of the forecasting system we implemented was the warm-start configuration of the data assimilation cycle, a setup that was made possible by close links with the operational center at FNMOC. The COAMPS model analysis cycle was initialized with the 12-h forecast from the previous model run, thus allowing the retention of much of the mesoscale and parameterized atmospheric structure from one run to the next (e.g., Hodur 1987, 1997). In contrast, at present (October 1998) most nonoperational forecasting uses a cold start procedure, that is, where the initialization uses another model forecast interpolated onto the mesoscale model grid for the first-guess fields [Mass and Kuo (1988), and http://www.mmm.ucar.edu/mm5/mm5forecast/sites.html]. This can result in poor forecasts of parameterized fields such as precipitation, while the model "spins up," as in the first case discussed. This should be a consideration in the planning of any field work support.

In conclusion, we would not hesitate to recommend the use of a specially tailored forecasting system for the detailed planning and operation of any meteorological or oceanographic field program. This comment is particularly germane for field programs aimed at observing events in a remote location, and that vary on the time- and space scales only a mesoscale forecast model could resolve. From our experience during the 1997 Labrador Sea Experiment, we would advocate that the numerical weather prediction be carried out at a stable home base, where a reliable data assimilation and analysis cycle can be implemented. A *careful* selection of model output can then be processed and transferred over the Internet to the field base, where on-site data visualization can then be used in the planning of scientific activities.

Acknowledgments. The Labrador Sea Deep Convection Experiment is supported by the Office of Naval Research. Numerical simulations were performed on the Cray C90 at NRL/FNMOC under the sponsorship of the 6.4 SPAWAR program directed by Capt. Charles Hopkins. We would like to thank all at the 53d Squadron of the USAF Reserve, and the St. John's Weather Centre. The daily weather summaries described in the paper were prepared by John Mavriyannakis, Mariusz Pagowski, Ian Renfrew, and Sudharshan Sathiyamoorthy. The postprocessing computer scripts were written and maintained by Vladimir Smirnov, and additional computing support was provided by Marco de la Cruz (all based at the University of Toronto). Figures 1 and 3 were redrawn by Khader Khan, and Fig. 7b was generously provided by Paris Vachon. The R/V *Knorr* surface state variable data were collected by a group led by Karl Bumke of the Institut für Meerskunde, University of Kiel, Kiel, Germany. We would also like to thank Keith Alverson, Mariusz Pagowski, and Sudharshan Sathiyamoorthy for their comments on this report.

References

Alpers, W., and B. Brümmer, 1994: Atmospheric boundary layer rolls observed by the synthetic aperture radar aboard the ERS-1 satellite. *J. Geophys. Res.,* **99,** 12 613–12 621.

Alverson, K., 1997: Mechanisms for lateral exchange with oceanic convection sites. *J. Phys. Oceanogr.,* **27,** 1436–1446.

Baker, N. L., 1992: Quality control for the U.S. Navy operational database. *Wea. Forecasting,* **7,** 250–261.

Bretherton, C. S., and R. Pincus, 1995: Cloudiness and marine boundary layer dynamics in the ASTEX Lagrangian experiments. Part I: Synoptic setting and vertical structure. *J. Atmos. Sci.,* **52,** 2707–2723.

Cherry-Garrad, A., 1922: *The Worst Journey in the World.* Carroll and Graf, 607 pp.

Cotton, W. R., G. Thompson, and P. W. Mielke, 1994: Real-time mesoscale prediction on workstations. *Bull. Amer. Meteor. Soc.,* **75,** 349–362.

Doyle, J. D., 1995: Coupled ocean wave/atmosphere mesoscale model simulations of cyclogenesis. *Tellus,* **47A,** 766–778.

Grossman, R. L., and A. K. Betts, 1990: Air-sea interaction during an extreme cold air outbreak from the eastern coast of the United States. *Mon. Wea. Rev.,* **118,** 324–342.

Hodur, R., 1987: Evaluation of a regional model with an update cycle. *Mon. Wea. Rev.,* **115,** 2702–2718.

——, 1997: The Naval Research Laboratory's Coupled Ocean/Atmosphere Mesoscale Prediction System (COAMPS). *Mon. Wea. Rev.,* **125,** 1414–1430.

Joly, A., and Coauthors, 1997: The Fronts and Atlantic Storms Experiment (FASTEX): Scientific objectives and experimental design. *Bull. Amer. Meteor. Soc.,* **78,** 1917–1940.

Killworth, P. D., 1983: Deep convection in the world ocean. *Rev. Geophys. Space Phys.,* **21,** 1–26.

Lab Sea Group, 1998: The Labrador Sea Deep Convection Experiment. *Bull. Amer. Meteor. Soc.,* **79,** 2033–2058.

Marshall, J., and F. Schott, 1999: Open ocean deep convection: Observations, theory and models. *Rev. Geophys.,* **37,** 1–64.

Mass, C. F., and Y.-H. Kuo, 1998: Regional real-time numerical weather prediction: Current status and future potential. *Bull. Amer. Meteor. Soc.,* **79,** 253–263.

Mellor, G. L., and T. Yamada, 1974: A hierarchy of turbulence closure models for planetary boundary layers. *J. Atmos. Sci.,* **31,** 1791–1809.

Powers, J. G., M. T. Stoelin, and W. S. Boyd, 1997: Distributed numerical weather prediction via satellite. *Bull. Amer. Meteor. Soc.*, **78,** 2755–2770.

Renfrew, I. A., and G. W. K. Moore, 1999: An extreme cold air outbreak over the Labrador Sea: Roll vortices and air–sea interaction. *Mon. Wea. Rev.*, in press.

Visbeck, M., J. Marshall, and H. Jones, 1996: Dynamics of isolated convective regions in the ocean. *J. Phys. Oceanogr.*, **26,** 1721–1734.

Warner, T. W., and N. L. Seaman, 1990: A real-time mesoscale numerical weather prediction system used for research, teaching and public service at the Pennsylvania State University. *Bull. Amer. Meteor. Soc.*, **71,** 792–805.